

Many-Body Density Matrices On a Two-Dimensional Square Lattice: Noninteracting and Strongly Interacting Spinless Fermions

Siew-Ann Cheong and Christopher L. Henley

Laboratory of Atomic and Solid State Physics, Cornell University, Ithaca, New York 14853-2501, USA

(Dated: February 8, 2020)

A common assumption in the quantum mechanics literature is that it is *always* possible to calculate a reduced density matrix starting from a given many-body wave function, *regardless* of the statistics of the particles involved. In this paper, we consider a lattice model of spinless fermions, and guide the reader through the subtlety of fermion signs, to arrive at a consistent definition for the density matrix of a cluster of sites, obtained by tracing out the degrees of freedom outside the cluster. To illustrate the practicality of such a definition in dimensions greater than one, we calculate numerically the cluster density matrix of a system of strongly-interacting spinless fermions with infinite nearest-neighbor repulsion on a square lattice, starting from the exactly-diagonalized ground-state wave functions of systems with up to 20 sites. To the best of our knowledge, this is the first paper in which cluster density matrices were calculated from exact diagonalizations of an extended system in the case of a *fermion* model. We then describe several averaging apparatus needed to reduce finite size effects in the numerics, so that a meaningful comparison can be made between the cluster density matrices of noninteracting and strongly-interacting spinless fermions.

I. INTRODUCTION

The density matrix is a very useful tool in the numerical study of interacting systems. Besides being used in the Density-Matrix Renormalization Group (DMRG)¹ and its higher-dimensional generalizations,² the density matrix is also used as a diagnostic tool in the Contractor Renormalization (CORE) method for numerical renormalization group in two dimensions,³ and forms the basis of a method to identify the order parameter related to a quasi-degeneracy of ground states.⁴

In previous work,¹⁰ we extended the results of Chung and Peschel⁵ to write the density matrix (DM) of a cluster of N_C sites cut out from a system of noninteracting spinless fermions in d dimensions as the exponential of a quadratic operator, called the pseudo-Hamiltonian, as it resembles the Hamiltonian of a noninteracting system. That result was then applied in numerical studies of noninteracting spinless fermions in one dimension, to better understand how the distribution of cluster DM eigenvalues scale with N_C , and to explore the possibility of designing truncation schemes based on the pseudo-Hamiltonian.⁶ We believe truncation schemes such as that described in Ref.6 will be helpful to the choice of basis states in renormalization groups such as CORE.

Thus, some questions motivating the present paper were: (i) does the density matrix of an interacting Fermi-liquid system resembles that of a noninteracting one? (ii) can we apply our exact result in Ref.10 to two dimensions as well as for one dimension? (iii) is it numerically practical to compute this sort of density matrix in a fermion system. To answer these questions, we investigated a spinless analog of the extended Hubbard model, given by

the Hamiltonian

$$H = -t \sum_{\langle i,j \rangle} c_i^\dagger c_j + V \sum_{\langle i,j \rangle} n_i n_j, \quad (1.1)$$

in the limit of $V \rightarrow \infty$, so that fermions are not allowed to be nearest neighbors of each other. This model is chosen because it has a rich zero-temperature phase diagram,⁷⁻⁹ where we find practically free fermions in the limit $\bar{n} \ll 1$, and an inert solid at half-filling $\bar{n} = \frac{1}{2}$. As the filling fraction approaches quarter-filling from below, $\bar{n} \rightarrow \frac{1}{4}^-$, the system becomes congested, highly correlated, but is nonetheless a Fermi liquid, perhaps with additional orders that are not clear in small systems. Slightly above quarter-filling, the dense fluid and inert solid coexists, while slightly below half-filling, the system is expected to support stable arrays of stripes.

To probe this rich variety of structures in the ground state at different filling fraction \bar{n} , we describe in Section II how the reduced DM of a small cluster, with the appropriate symmetry properties, can be calculated from a finite non-square system subject to twist boundary conditions. Then in Section III, we investigate in great details the cluster DM spectra of the noninteracting system, particularly on how to handle finite size effects in the numerics, for comparison with the cluster DM spectra of a strongly-interacting system, presented in Section IV. Finally, in Section V, we summarized our findings, and discuss the prospects of designing an Operator-Based DM Truncation Scheme for interacting systems, at some, if not at all, filling fractions.

II. FORMULATION

In this section, we formulate the theoretical and numerical tools needed for our investigations into the cluster DM spectra of noninteracting and strongly-interacting systems of spinless fermions in two dimensions. In Section II A, we show how the DM of a small cluster embedded within a larger, but still finite, system can be calculated by tracing out degrees of freedom external to the cluster, starting from the ground-state wave function of the system, obtained through exact diagonalization. In Section II B, we describe how our finite systems can be defined with nonsquare periodic boundary conditions, and how we make use of the translational invariance of both noninteracting and strongly-interacting models to reduce the computational efforts in exact diagonalization. In Section II C, we describe several averaging apparatus required to obtain a handle on the infinite-system limit spectra of the cluster DM, and then in Section II D, we describe a classification scheme for the one-particle and multi-particle eigenstates of the cluster DM that makes the symmetry of the underlying square lattice explicit.

A. Cluster Density Matrix

The DM ρ_C of a cluster cut out from a larger system is a density operator which gives the expectation

$$\langle \Psi | A | \Psi \rangle = \langle A \rangle = \text{Tr}_C \rho_C A \quad (2.1)$$

for any observable A local to the cluster, when the larger system is in its ground state $|\Psi\rangle$. It is commonly assumed that the cluster DM ρ_C can be calculated from the ground-state DM

$$\rho = |\Psi\rangle \langle \Psi| \quad (2.2)$$

of the system, by tracing out degrees of freedom outside of the cluster. We write this as

$$\rho_C = \text{Tr}_E \rho, \quad (2.3)$$

where the subscript E denotes a trace over environmental degrees of freedom. In the following subsections, we shall show that it is possible to define an object ρ_C which is consistent with both (2.1) and (2.3).

1. Configurational Basis States

Since a cluster is a collection of sites identified in real space, it is natural to choose as a many-body basis the real-space configurations. The following derivation does not depend on dimensionality, but we shall assume a two-dimensional lattice for the sake of concreteness.

For a finite two-dimensional system with N sites, we label the sites $j = 1$ through $j = N$, so that for any

pair of sites (x_{j_1}, y_{j_1}) and (x_{j_2}, y_{j_2}) , we have $x_{j_1} \leq x_{j_2}$ and $y_{j_1} < y_{j_2}$ if $j_1 < j_2$. We then distinguish between sites within the cluster, of which there are N_C of them, $(x_{j_1^C}, y_{j_1^C}), (x_{j_2^C}, y_{j_2^C}), \dots, (x_{j_{N_C}^C}, y_{j_{N_C}^C})$, and sites outside of the cluster, of which there are $N_E = N - N_C$ of them, $(x_{j_1^E}, y_{j_1^E}), (x_{j_2^E}, y_{j_2^E}), \dots, (x_{j_{N_E}^E}, y_{j_{N_E}^E})$. We think of the N_E sites outside the cluster as constituting the *environment* to the cluster.

We work with the configuration basis states $|\mathbf{j}\rangle = |j_1 j_2 \dots j_P\rangle$, where $j_1 < \dots < j_P$ are the P occupied sites in the system. These can be thought of as a direct product of the configuration basis states of the cluster $|\mathbf{l}\rangle = |l_1 l_2 \dots l_{P_C}\rangle$, where $l_1 < \dots < l_{P_C}$ are the P_C occupied sites within the cluster, and the configuration basis states of the environment $|\mathbf{m}\rangle = |m_1 m_2 \dots m_{P_E}\rangle$, where $m_1 < \dots < m_{P_E}$ are the $P_E = P - P_C$ occupied sites in the environment. Here, we have the occupied sites of the system $\{j_1, \dots, j_P\} = \{l_1, \dots, l_{P_C}\} \cup \{m_1, \dots, m_{P_E}\}$ being the union of the occupied sites in the cluster and in the environment, with the site indices l and m resorted in ascending order to give the site indices j .

2. Matrix Elements

The ground-state wave function of the system can be written as

$$|\Psi\rangle = \sum_{\mathbf{j}} \Psi_{\mathbf{j}} |\mathbf{j}\rangle = \sum_{\mathbf{j}} \Psi_{\mathbf{j}} c_{j_1}^\dagger \dots c_{j_P}^\dagger |0\rangle, \quad (2.4)$$

in terms of the configuration basis of the system, where $\Psi_{\mathbf{j}}$ is the amplitude associated with configuration $|\mathbf{j}\rangle$, and c_j, c_j^\dagger are fermion annihilation and creation operators acting on the site (x_j, y_j) , or as

$$\begin{aligned} |\Psi\rangle &= \sum_{\mathbf{l}} \sum_{\mathbf{m}} (-1)^{f(\mathbf{j}, \mathbf{l}, \mathbf{m})} \Psi_{\mathbf{l}, \mathbf{m}} |\mathbf{l}\rangle |\mathbf{m}\rangle \\ &= \sum_{\mathbf{l}} \sum_{\mathbf{m}} (-1)^{f(\mathbf{j}, \mathbf{l}, \mathbf{m})} \Psi_{\mathbf{l}, \mathbf{m}} \times \\ &\quad c_{m_1}^\dagger \dots c_{m_{P_E}}^\dagger c_{l_1}^\dagger \dots c_{l_{P_C}}^\dagger |0\rangle, \end{aligned} \quad (2.5)$$

in terms of the direct product of configuration bases of the cluster and the environment, where c_l and c_l^\dagger are fermion annihilation and creation operators acting on site (x_l, y_l) within the cluster, and c_m and c_m^\dagger are fermion annihilation and creation operators acting on site (x_m, y_m) within the environment. In (2.5), the amplitude $\Psi_{\mathbf{l}, \mathbf{m}} = \Psi_{\mathbf{j}}$ is taken directly from the expansion in (2.4), while the factor $(-1)^{f(\mathbf{j}, \mathbf{l}, \mathbf{m})}$ accounts for the fermion sign incurred when we reorder the operator product $c_{m_1}^\dagger \dots c_{m_{P_E}}^\dagger c_{l_1}^\dagger \dots c_{l_{P_C}}^\dagger$ to get the operator product $c_{j_1}^\dagger \dots c_{j_P}^\dagger$.

Similarly, the ground-state DM in (2.2) can be written as

$$\rho = \sum_{\mathbf{j}} \sum_{\mathbf{j}'} \Psi_{\mathbf{j}} \Psi_{\mathbf{j}'}^* c_{j_1}^\dagger \dots c_{j_P}^\dagger |0\rangle \langle 0| c_{j'_1} \dots c_{j'_P} |0\rangle, \quad (2.6)$$

using the system-wide configuration basis, or as

$$\rho = \sum_{\mathbf{l}, \mathbf{m}} \sum_{\mathbf{l}', \mathbf{m}'} (-1)^{f(\mathbf{j}; \mathbf{l}, \mathbf{m}) + f(\mathbf{j}'; \mathbf{l}', \mathbf{m}')} \Psi_{\mathbf{l}, \mathbf{m}} \Psi_{\mathbf{l}', \mathbf{m}'}^* \times \\ c_{m_1}^\dagger \cdots c_{m_{P_E}}^\dagger c_{l_1}^\dagger \cdots c_{l_{P_C}}^\dagger |0\rangle \times \\ \langle 0| c_{l'_{P'_C}} \cdots c_{l'_1} c_{m'_{P'_E}} \cdots c_{m'_1}, \quad (2.7)$$

using the direct-product basis between cluster configurations and environment configurations.

Using (2.7), the ground-state expectation $\langle A \rangle = \text{Tr } \rho A$ of an observable A can be written as

$$\sum_{\mathbf{l}'', \mathbf{m}''} \sum_{\mathbf{l}, \mathbf{m}} \sum_{\mathbf{l}', \mathbf{m}'} (-1)^{f_{\mathbf{j}} + f_{\mathbf{j}''}} \Psi_{\mathbf{l}, \mathbf{m}} \Psi_{\mathbf{l}', \mathbf{m}'}^* \times \\ \langle 0| c_{l''_{P''_C}} \cdots c_{l''_1} c_{m''_{P''_E}} \cdots c_{m''_1} c_{m_1}^\dagger \cdots c_{m_{P_E}}^\dagger c_{l_1}^\dagger \cdots c_{l_{P_C}}^\dagger |0\rangle \times \\ \langle 0| c_{l'_{P'_C}} \cdots c_{l'_1} c_{m'_{P'_E}} \cdots c_{m'_1} A c_{m''_1}^\dagger \cdots c_{m''_{P''_E}}^\dagger c_{l''_1}^\dagger \cdots c_{l''_{P''_C}}^\dagger |0\rangle, \quad (2.8)$$

which is a sum of products of two expectations. In the first expectation

$$\langle 0| c_{l''_{P''_C}} \cdots c_{l''_1} c_{m''_{P''_E}} \cdots c_{m''_1} c_{m_1}^\dagger \cdots c_{m_{P_E}}^\dagger c_{l_1}^\dagger \cdots c_{l_{P_C}}^\dagger |0\rangle, \quad (2.9)$$

if $\mathbf{m}'' \neq \mathbf{m}$ because $P''_E \neq P_E$, then we would have one or more unbalanced annihilation operators which can be pushed right all the way through to annihilate $|0\rangle$, or one or more unbalanced creation operator which can be pushed left all the way through to annihilate $\langle 0|$. Alternatively, we have may have $P''_E = P_E$ but $\mathbf{m}'' \neq \mathbf{m}$, in which case the creation operators in \mathbf{m} do not match up with the annihilation operators in \mathbf{m}'' . Only when $\mathbf{m}'' = \mathbf{m}$ is this expectation nonzero, which can be simplified as

$$\langle 0| c_{l''_{P''_C}} \cdots c_{l''_1} c_{l_1}^\dagger \cdots c_{l_{P_C}}^\dagger |0\rangle \delta_{\mathbf{m}, \mathbf{m}''}. \quad (2.10)$$

In the second expectation

$$\langle 0| c_{l'_{P'_C}} \cdots c_{l'_1} c_{m'_{P'_E}} \cdots c_{m'_1} A c_{m''_1}^\dagger \cdots c_{m''_{P''_E}}^\dagger c_{l''_1}^\dagger \cdots c_{l''_{P''_C}}^\dagger |0\rangle, \quad (2.11)$$

we note that if A is an observable acting only within the cluster, it can be written as a sum of products of creation and annihilation operators within the cluster. Whatever the fermion sign we incur when anticommuting $c_{m''_1}^\dagger \cdots c_{m''_{P''_E}}^\dagger$ through A , this expectation will vanish unless $\mathbf{m}'' = \mathbf{m}'$. Consequently, we have $P''_E = P'_E$, hence $P''_C = P'_C$, and the only terms in the operator expansion of A that contributes nontrivially to the expectation are those containing a balanced product of creation and annihilation operators. Therefore, in computing the expectation of A , we can simply bring $c_{m'_1}^\dagger \cdots c_{m''_{P''_E}}^\dagger$ across A as if they commute with one another, giving us

$$\langle 0| c_{l'_{P'_C}} \cdots c_{l'_1} A c_{l''_1}^\dagger \cdots c_{l''_{P''_C}}^\dagger |0\rangle \delta_{\mathbf{m}', \mathbf{m}''}. \quad (2.12)$$

With these two observations, we realized that the expectation of an observable A local to the cluster can be written as (2.1), provided we define the fermion cluster DM ρ_C to be

$$\rho_C = \sum_{\mathbf{l}, \mathbf{l}'} \sum_{\mathbf{m}, \mathbf{m}'} (-1)^{f(\mathbf{j}; \mathbf{l}, \mathbf{m}) + f(\mathbf{j}'; \mathbf{l}', \mathbf{m}')} \times \\ \Psi_{\mathbf{l}, \mathbf{m}} \Psi_{\mathbf{l}', \mathbf{m}'}^* \delta_{\mathbf{m}, \mathbf{m}'} \times \\ c_{l_1}^\dagger \cdots c_{l_{P_C}}^\dagger |0\rangle \langle 0| c_{l'_{P'_C}} \cdots c_{l'_1}, \quad (2.13)$$

whose matrix elements are

$$\langle \mathbf{l} | \rho_C | \mathbf{l}' \rangle = \sum_{\mathbf{m}} \sum_{\mathbf{m}'} (-1)^{f(\mathbf{j}; \mathbf{l}, \mathbf{m}) + f(\mathbf{j}'; \mathbf{l}', \mathbf{m}')} \times \\ \Psi_{\mathbf{l}, \mathbf{m}} \Psi_{\mathbf{l}', \mathbf{m}'}^* \delta_{\mathbf{m}, \mathbf{m}'}. \quad (2.14)$$

Note that to get from (2.11) to (2.12), and thus furnish the definition in (2.13) for the cluster DM that is consistent with both (2.1) and (2.3), we need to be able to commute all products of environment operators through the observable A , so that our definition for ρ_C in (2.13) does not depend on which observable A we are looking into. For this, we actually needed to worry about two things: (i) there are no non-trivial local observables A with $\langle A \rangle \neq 0$ for which we cannot commute *all* products of environment operators through; and (ii) there are trivial local observables A with $\langle A \rangle = 0$ for which we would end up calculating a non-zero expectation.

We find that these two conditions are satisfied for ground states with definite particle number, which is what we would get from exact diagonalization. Moreover, it turns out that these two conditions are also true for a BCS ground state, which has indefinite particle number. For all non-trivial observables, we would still receive contributions to their expectations only from configurations for which $\mathbf{m}'' = \mathbf{m}'$, i.e. $P''_E = P'_E$. However, because the wave function consists of a linear superposition of terms with an even number of fermions, it is possible to receive nonzero contributions from those cluster configurations \mathbf{l}'' and \mathbf{l}' such that $P''_C - P'_C$ is a nonnegative even number. For example, the anomalous local observable $A = c_{j'_1}^\dagger c_{j'_2}^\dagger$ will receive non-zero contributions from those cluster configurations \mathbf{l}'' and \mathbf{l}' with $P'_C - P''_C = 2$. In any case, anomalous local observables A must still consist of a sum of products of an even number of fermion operators, though not necessarily all balanced, and we can therefore commute all products $c_{m''_1}^\dagger \cdots c_{m''_{P''_E}}^\dagger$ of environment operators through A to arrive at (2.12).

If, however, the ground-state wave function is a superposition of terms containing both even and odd number of particles, then there will be *some* anomalous local observables A containing products of odd numbers of fermion operators, which has non-zero ground-state expectation. In such cases, the cluster DM is not a physically meaningful description of the quantum-mechanical

state of the cluster, because if we calculate its matrix elements using (2.14), we would end up with the wrong expectations for many anomalous observables. Fortunately, ground states of this nature do not occur frequently, if at all, in physically meaningful models, so we do not need to be unduly worried about this scenario.

3. Computational Implementation

To determine the computational complexity involved in calculating the cluster DM numerically, let us denote by $D(P)$ the size of the system Hilbert space with P particles, $D_C(P_C)$ the size of the cluster Hilbert space with P_C particles, and $D_E(P_C)$ the size of the environment Hilbert space with $P_E = P - P_C$ particles. Noting that there can be no matrix elements between cluster configurations with different number of particles, we calculate each P_C sector of the cluster DM separately. To keep our notations compact, let us drop the P and P_C dependences in $D(P)$, and $D_{C,E}(P_C)$ respectively from this point onwards, and reinstate these dependences only when necessary. Readers are referred to Ref.11 for more technical details on the computational implementation of this trace-down calculation of the cluster DM.

The naive way to compute the cluster DM matrix elements, after looking at the formula (2.14), would be to immediately start nested for loops in \mathbf{l} and \mathbf{l}' , each running over D_C indices. For each pair of cluster configurations $|\mathbf{l}\rangle$ and $|\mathbf{l}'\rangle$, one would need to then determine which of the P -particle configurations $|\mathbf{j}\rangle$ contain the two cluster configurations. This involves running through the D configurations in the system Hilbert space, and for each configuration, comparing the P occupied sites with the P_C occupied sites in the cluster configurations $|\mathbf{l}\rangle$ and $|\mathbf{l}'\rangle$. The computational effort incurred for this matching is thus $O(DP)$. Two vectors of indices, \mathbf{i} , whose entries are the indices of system configurations $|\mathbf{j}\rangle$ giving cluster configuration $|\mathbf{l}\rangle$, and \mathbf{i}' , whose entries are the indices of system configurations $|\mathbf{j}\rangle$ giving cluster configuration $|\mathbf{l}'\rangle$, are obtained. The lengths of these index vectors vary, but are of $O(D_E)$. One can then compare the two index vectors, at a computational cost of $O(D_E^2)$, to find which pairs of system configurations giving cluster configurations $|\mathbf{l}\rangle$ and $|\mathbf{l}'\rangle$ share the same environment configuration. Following this, one can sum over the amplitude of such pairs, at a computational cost of $O(D_E)$, to obtain the cluster DM matrix element $\langle \mathbf{l} | \rho_C | \mathbf{l}' \rangle$. For this naive algorithm, the net computational effort is on the order of $D_C^2(DP + D_E^2 + D_E) \sim D_C^2(DP + D_E^2)$.

Alternatively, we can note that the formula (2.14) for the matrix element $\langle \mathbf{l} | \rho_C | \mathbf{l}' \rangle$ of the cluster DM look like an inner product between two vectors, and pre-sort the ground-state wave function. Running through the D system configurations, we determine, at a computational cost of P for each system configuration $|\mathbf{j}\rangle$, what cluster configuration $|\mathbf{l}\rangle$ and environment configuration $|\mathbf{m}\rangle$

it contains. We must then search through the cluster and environment Hilbert spaces to determine what the indices of $|\mathbf{l}\rangle$ and $|\mathbf{m}\rangle$ are in their corresponding Hilbert spaces. This incurs a computational effort on the order of $D_C P_C$ and $D_E P_E$ respectively. Once these indices are determined, the amplitudes in the ground-state wave function can be organized into a $D_C \times D_E$ matrix. The net computational expenditure is thus on the order of $D(P + D_C P_C + D_E P_E) \sim D(D_C P_C + D_E P_E)$. After sorting the ground-state wave function, we can then start nested for loops in \mathbf{l} and \mathbf{l}' , each running over D_C indices, to evaluate the matrix element $\langle \mathbf{l} | \rho_C | \mathbf{l}' \rangle$ as the inner product between two vectors of length D_E . This trace-down stage incurs a computational cost of $O(D_C^2 D_E)$. Overall, the computational cost is on the order of $D(D_C P_C + D_E P_E) + D_C^2 D_E$.

For models allowing nearest-neighbor occupation, the system Hilbert space is the direct product of the cluster Hilbert space and the environment Hilbert space, i.e. $D = D_C D_E$. Since the number P of particles is small in any reasonable exact diagonalization, we can treat it as a $O(1)$ constant. For small clusters, the size D_C of the cluster Hilbert space will also be small, so that the size D_E of the environment Hilbert space will be comparable in magnitude to D . With these considerations, we find that the computational cost for the naive algorithm is $O(D D_C^2 + D_C^2 D_E^2) \sim O(D^2)$, while the computational cost for the inner-product algorithm with pre-sorting is $O(D + D D_E + D_E) \sim O(D^2)$. The efficiency of the two algorithms therefore depend on the prefactors.

For a model such as (1.1), where nearest-neighbor occupation is forbidden, the system Hilbert space is smaller than the direct product of the cluster Hilbert space and the environment Hilbert space, i.e. $D < D_C D_E$. Given again that P and D_C are small numbers, the computational cost for the two algorithms are essentially determined by the ratio $D_C D_E / D$. This ratio is strongly dependent on the dimensionality of the problem: the superfluous configurations generated by the direct product of the cluster Hilbert space and the environment Hilbert space are invalid because they contain nearest-neighbor sites, right at the boundary between the cluster and its environment, which are occupied. In one dimension, the number of superfluous configurations is small, because the boundary between the cluster and its environment consists only of two bonds, whatever the size N_C of the cluster. In two dimensions, the boundary between the cluster and its environment is a line cutting roughly $\sqrt{N_C}$ bonds. The number of superfluous configurations is then proportional to $\exp(\alpha_2 \sqrt{N_C})$, where α_2 is a constant prefactor which depends on the shape of the cluster. In d dimensions, the number of boundary bonds is on the order of $N_C^{(d-1)/d}$, and the number of superfluous states is proportional to $\exp(\alpha_d N_C^{(d-1)/d})$. Therefore, in dimensions greater than one, $D_C D_E$ become increasingly larger than D as N_C is increased, and the inner-product algo-

rithm with pre-sorting, which involves only one power of $D_C D_E$, is more efficient than the naive algorithm, which involves $(D_C D_E)^2$.

B. System Definition and Translational Invariance

For noninteracting spinless fermions on an infinite square lattice, it is possible to compute the cluster DM ρ_C starting from the Fermi sea ground state, through the evaluation and diagonalization of G_C . For an interacting system, we need to compute ρ_C starting from ρ in (2.2), the latter we obtain through exact diagonalization on a finite system. We define the a finite system relative to the infinite square lattice in terms of the lattice vectors \mathbf{R}_1 and \mathbf{R}_2 , as shown in Fig. 1, such that $N = \hat{\mathbf{z}} \cdot (\mathbf{R}_1 \times \mathbf{R}_2) = R_{1x}R_{2y} - R_{2x}R_{1y} > 0$ is the number of lattice sites within the system.

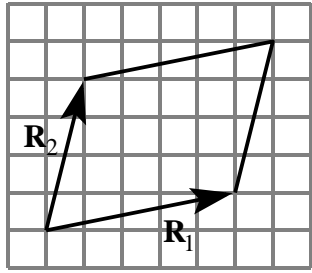


FIG. 1: Definition of system to be exactly diagonalized in terms of the lattice vectors \mathbf{R}_1 and \mathbf{R}_2 . We shall denote such a system as $\mathbf{R}_1 \times \mathbf{R}_2$. In this example shown, the system is $(5, 1) \times (1, 4)$.

If we impose periodic boundary condition such that $\mathbf{R} + m\mathbf{R}_1 + n\mathbf{R}_2 \equiv \mathbf{R}$, then in the exact diagonalization to obtain $|\Psi\rangle$ we can take advantage of translational invariance through the use of the Bloch states

$$|\mathbf{j}_0, \mathbf{k}\rangle = \frac{1}{\sqrt{N}} \sum_{\mathbf{R}} e^{-i\mathbf{k}\cdot\mathbf{R}} T_{\mathbf{R}} |\mathbf{j}_0\rangle \quad (2.15)$$

as our computational basis.⁸ In this Bloch state, the configurations $\{T_{\mathbf{R}} |\mathbf{j}_0\rangle\}$ are all related to the generating configuration $|\mathbf{j}_0\rangle$ by the lattice translations $T_{\mathbf{R}}$ associated with displacement \mathbf{R} , while \mathbf{k} are wave vectors allowed by the boundary conditions. Any configuration within the collection of translationally-related configurations $\{T_{\mathbf{R}} |\mathbf{j}_0\rangle\}$ can serve as the generating configuration, but we pick the one with the least sum of indices of occupied sites.

Working with finite non-square systems introduces several complications. First of all, we sometimes end up with degenerate ground states which suffer from symmetry-breaking not found in the true infinite-system ground state. However, because the point symmetry group of our non-square finite system is only a subgroup of the square

lattice point symmetry group, the finite-system ground-state manifold is not invariant under all square lattice symmetry operations. Thirdly, when working with finite systems, we introduce systematic deviations which are collectively known as *finite size effects*. We identify the three primary sources of finite size effects as (i) finite domain effect, which has to do with the fact that the small set of discrete wave vectors allowed are not adequately representative of the continuous set of wave vectors on the infinite square lattice; (ii) shell effect, which has to do with the fact that the set of discrete wave vectors allowed are organized by symmetry into shells in reciprocal space, each of which can be partially or fully filled in the many-body ground state; and (iii) shape effect, which has to do with the detailed shape of the non-square system we introduced.

C. Averaging

1. Degeneracy Averaging

To eliminate these numerical artefacts, we adopted three averaging devices. First, we average over the D_0 -fold degenerate ground-state manifold. Our first motivation for doing so is as follows: if \mathcal{G} is the point symmetry group of the square lattice, and its subgroup G is the point symmetry group of the $\mathbf{R}_1 \times \mathbf{R}_2$ system, then we will find that the cluster density matrices

$$\rho_{C,i} = \text{Tr}_E |\Psi_i\rangle \langle \Psi_i|, \quad (2.16)$$

one for each wave function Ψ_i within the D_0 -fold degenerate ground-state manifold, are not invariant under G , much less \mathcal{G} . We remove this artificial symmetry breaking by calculating the degeneracy-averaged cluster DM

$$\rho_C = \frac{1}{D_0} \sum_{i=1}^{D_0} \rho_{C,i} \quad (2.17)$$

over the cluster density matrices $\rho_{C,i}$ within the ground-state manifold. This degeneracy-averaged cluster DM is invariant under G .

A second motivation for such a mode of averaging over the degenerate ground-state manifold of the finite system is that thermodynamically, given the pure state density matrices $\rho_{C,i}$, with energy eigenvalue E_i , we typically construct the canonical ensemble DM as

$$\rho_C(\beta) = Z^{-1}(\beta) \sum_i e^{-\beta E_i} \rho_{C,i}, \quad (2.18)$$

where $Z(\beta) = \sum_i e^{-\beta E_i}$ is the canonical partition function. States within a degenerate manifold have the same energy, and therefore contribute equally to the thermodynamic DM $\rho_C(\beta)$. In the limit of $\beta \rightarrow \infty$, the usual thermodynamic argument is that pure states decouple from one another, and we treat their respective density

matrices independently, except for those states which are degenerate. Because they appear with the same Boltzmann weight whatever the inverse temperature is, we should still treat the uniform combination instead of the individual density matrices in the limit of $\beta \rightarrow \infty$,

2. Orientation Averaging

The second averaging device involves an average over the orientation of the finite non-square system relative to the underlying square lattice. This averaging restores the \mathcal{G} -symmetry to the averaged ground state. In principle, this requires us to compute ρ_C for a group of four systems: $(R_{1x}, R_{1y}) \times (R_{2x}, R_{2y})$, $(R_{2y}, R_{2x}) \times (R_{1y}, R_{1x})$, $(R_{1x}, -R_{1y}) \times (-R_{2x}, R_{2y})$ and $(R_{2y}, -R_{2x}) \times (-R_{1y}, R_{1x})$.

However, if the cluster whose DM we are calculating is invariant under the action of \mathcal{G} , this averaging can be achieved by computing

$$\bar{\rho}_C = \frac{1}{D(\mathcal{G})} \sum_{g \in \mathcal{G}} U_g \rho_C U_g^\dagger, \quad (2.19)$$

where $g \in G$ is a point group transformation of the square lattice, U_g is the unitary transformation of the cluster Hilbert space associated with g , and $D(\mathcal{G})$ is the order of \mathcal{G} .

3. Twist Boundary Conditions Averaging

After these two averagings, the cluster DM has the full symmetry (including translations) of the underlying square lattice, but finite size effects remain. We eliminate these as much as we can¹¹ with the third averaging device, twist boundary conditions averaging.¹² The usual way to implement twist boundary conditions is to work in the *boundary gauge*, keeping the Hamiltonian unchanged, and demanding that

$$c_{\mathbf{R}+\mathbf{R}_1} = e^{-i\phi \cdot \mathbf{R}_1} c_{\mathbf{R}}, \quad c_{\mathbf{R}+\mathbf{R}_2} = e^{-i\phi \cdot \mathbf{R}_2} c_{\mathbf{R}}, \quad (2.20)$$

where \mathbf{R}_1 and \mathbf{R}_2 are the lattice vectors defining our finite system, $\mathbf{R} = (R_x, R_y)$ is a site within the system, and $\phi = (\phi_x, \phi_y)$ is the twist vector parametrizing the twist boundary conditions.

In choice of gauge (2.20), the Hamiltonian (1.1) is not manifestly invariant under translations. However, we can continue to block-diagonalize it using the Bloch basis states defined in (2.15), provided the set of allowed wave vectors \mathbf{k} are shifted relative to \mathbf{k}_0 for the usual periodic boundary conditions by the twist vector ϕ , i.e.

$$\mathbf{k} = \mathbf{k}_0 + \phi. \quad (2.21)$$

The other natural way to implement twist boundary conditions is in the *bond gauge*, where we make the sub-

stitution

$$c_{\mathbf{R}} \rightarrow e^{-i\mathbf{R} \cdot \phi} c_{\mathbf{R}} \quad (2.22)$$

in the Hamiltonian, but demand that

$$c_{\mathbf{R}+\mathbf{R}_1} = c_{\mathbf{R}}, \quad c_{\mathbf{R}+\mathbf{R}_2} = c_{\mathbf{R}}, \quad (2.23)$$

where \mathbf{R}_1 and \mathbf{R}_2 are the lattice vectors defining our finite system. Now the Hamiltonian (1.1) is manifestly invariant under translations, and we can block-diagonalize it using the Bloch basis states defined in (2.15), with the same set of allowed wave vectors $\mathbf{k} = \mathbf{k}_0$ as for the usual periodic boundary conditions.

Exact diagonalization can be performed in any gauge, but we chose to do it in the bond gauge, because in this gauge, the Bloch basis states $|\mathbf{j}_0, \mathbf{k}\rangle$ defined in (2.15) can be used as is to block diagonalize the Hamiltonian at all twist vectors ϕ . This gives us the ground-state wave function $|\Psi(\text{bond})\rangle$ in the bond gauge. In the boundary gauge, or any other gauges, appropriate gauge transformations must be applied to $|\mathbf{j}_0, \mathbf{k}\rangle$ before we can use this Bloch basis to block diagonalize the Hamiltonian. Because of this, the computational cost for exact diagonalization incurred in the bond gauge is fractionally lower than in other gauges.

We can also calculate the correlation functions $\langle \tilde{O}(\mathbf{R}) \tilde{O}'(\mathbf{R} + \Delta\mathbf{R}) \rangle$ (of which the cluster DM is a function of) in any gauge, with appropriately-defined covariant observables $\tilde{O} = U O U^\dagger$, where O are the ‘physical’ observables we would use when there is no twist in the boundary conditions. In the boundary gauge, these covariant observables $\tilde{O} = O$ and $\tilde{O}' = O'$ are particularly simple, except when the displacement vector $\Delta\mathbf{R}$ crosses the boundaries of our system. For our purpose of calculating the cluster DM, this situation occurs only when the cluster itself straddle the system boundaries. Therefore, with the cluster properly nested within the system, we chose to perform twist boundary conditions averaging in the boundary gauge.

In the boundary gauge, the cluster DM is obtained by tracing down the ground-state wave function $|\Psi(\text{boundary})\rangle$. We can get this wave function from $|\Psi(\text{bond})\rangle$ by applying the gauge transformation

$$\varphi : |\mathbf{n}\rangle \rightarrow e^{-i \sum_{\mathbf{R}} n_{\mathbf{R}} \mathbf{R} \cdot \phi} |\mathbf{n}\rangle, \quad (2.24)$$

where $|\mathbf{n}\rangle$ is an occupation number basis state, with occupation $n_{\mathbf{R}}$ on site \mathbf{R} .

Now, averaging over twist vectors ϕ is the same as integrating over the Brillouin Zone, so we perform twist boundary conditions averaging over a uniform grid of Monkhorst-Pack points with order q .¹³ For rectangular systems $(L_x, 0) \times (0, L_y)$, the First Brillouin Zone is sampled by varying the two independent twist angles between $-\pi/L_x \leq \phi_x < +\pi/L_x$ and $-\pi/L_y \leq \phi_y < +\pi/L_y$. For non-square systems, the two independent twist angles ϕ_1 and ϕ_2 are defined by

$$e^{i\phi \cdot \mathbf{R}_1} = e^{i\phi_1}, \quad e^{i\phi \cdot \mathbf{R}_2} = e^{i\phi_2}. \quad (2.25)$$

The twist vector ϕ is then related to the independent twist angles $-\pi \leq \phi_1 < +\pi$ and $-\pi \leq \phi_2 < +\pi$ by

$$\phi = \frac{\phi_1}{2\pi} \mathbf{Q}_1 + \frac{\phi_2}{2\pi} \mathbf{Q}_2, \quad (2.26)$$

where

$$\mathbf{Q}_1 = \frac{2\pi}{N} (R_{2y}, -R_{2x}), \quad \mathbf{Q}_2 = \frac{2\pi}{N} (-R_{1y}, R_{1x}) \quad (2.27)$$

are the primitive reciprocal lattice vectors of our non-square system. For such systems, the First Brillouin Zone is a parallelogram on the ϕ_x - ϕ_y plane, so the uniform grid of Monkhorst-Pack points are imposed on the square domain $(-\pi, +\pi) \times (-\pi, +\pi)$ on the ϕ_1 - ϕ_2 plane instead.

D. Classifying States of the Cluster

The point symmetry group of the square lattice is the dihedral group D_4 , which has eight elements.¹⁴ The five irreducible representations of this group are A_1 , A_2 , B_1 , B_2 and E . For the cross-shaped cluster shown in Fig. 2, there is a one-to-one correspondence between these five irreducible representations and the one-particle states, but instead of labeling these one-particle states as $|A_1\rangle$, $|A_2\rangle$, $|B_1\rangle$, $|B_2\rangle$ and $|E\rangle$, we adopt an angular momentum-like notation,

$$\begin{aligned} |s_+\rangle &= |A_1\rangle = \frac{1}{\sqrt{5}}(1, 1, 1, 1, 1), \\ |s_-\rangle &= |A_2\rangle = \frac{1}{\sqrt{5}}(1, 1, -1, 1, 1), \\ |p_x\rangle &= |B_1\rangle = \frac{1}{\sqrt{2}}(1, 0, 0, 0, -1), \\ |p_y\rangle &= |B_2\rangle = \frac{1}{\sqrt{2}}(0, 1, 0, -1, 0), \\ |d\rangle &= |E\rangle = \frac{1}{2}(1, -1, 0, -1, 1). \end{aligned} \quad (2.28)$$

that would make clear the structure of these one-particle states. We find it more convenient to work with the one-particle states

$$\begin{aligned} |s\rangle &= \frac{1}{\sqrt{2}}|s_+\rangle + \frac{1}{\sqrt{2}}|s_-\rangle = \frac{1}{2}(1, 1, 0, 1, 1), \\ |\bar{s}\rangle &= (0, 0, 1, 0, 0), \\ |p_+\rangle &= \frac{1}{\sqrt{2}}|p_x\rangle + \frac{i}{\sqrt{2}}|p_y\rangle = \frac{1}{2}(1, i, 0, -i, -1), \\ |p_-\rangle &= \frac{1}{\sqrt{2}}|p_x\rangle - \frac{i}{\sqrt{2}}|p_y\rangle = \frac{1}{2}(1, -i, 0, i, -1). \end{aligned} \quad (2.29)$$

For a cluster DM possessing the full point group symmetry of the square lattice, the one-particle state $|d\rangle$ is constrained by symmetry to always be an eigenstate of ρ_C . We call its weight w_d . Furthermore, the one-particle states $|p_x\rangle$ and $|p_y\rangle$ are also equivalent under the square lattice symmetry, and hence their weights w_{p_x} and w_{p_y} are equal. We call this doubly-degenerate one-particle weight w_p . On the other hand, the s one-particle eigenstates of ρ_C are in general not $|s_+\rangle$, $|s_-\rangle$ or $|s\rangle$, $|\bar{s}\rangle$, but some admixture of the form

$$\begin{aligned} |s_1\rangle &= \cos \theta |s\rangle + \sin \theta |\bar{s}\rangle, \\ |s_2\rangle &= -\sin \theta |s\rangle + \cos \theta |\bar{s}\rangle. \end{aligned} \quad (2.30)$$

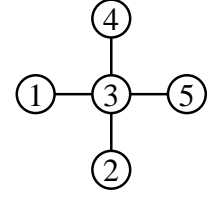


FIG. 2: The five-site, cross-shaped cluster whose cluster DM we are interested in calculating for both a system of noninteracting, as well as strongly-interacting spinless fermions.

We call their corresponding weights w_{s_1} and w_{s_2} respectively.

We can then extend this angular-momentum-like notation to multi-particle states of the cluster. Though the quantum numbers used to label the one-particle states are, strictly speaking, not angular momentum quantum numbers, we apply the rules of angular momenta addition as if they were to write down the angular-momentum-like quantum numbers for the multi-particle states. For example, for the two-particle states of the cluster, we have

$$\begin{aligned} |S\rangle &= |p_+p_-\rangle, \quad |S'\rangle = |s\bar{s}\rangle, \\ |P_+\rangle &= |sp_+\rangle, \quad |P'_+\rangle = |\bar{s}p_+\rangle, \quad |P''_+\rangle = |p_-d\rangle, \\ |P_-\rangle &= |sp_-\rangle, \quad |P'_-\rangle = |\bar{s}p_-\rangle, \quad |P''_-\rangle = |p_+d\rangle, \\ |D\rangle &= |sd\rangle, \quad |D'\rangle = |\bar{s}d\rangle. \end{aligned} \quad (2.31)$$

III. NONINTERACTING SYSTEM

In preparation for our main calculations on the strongly-interacting system, we investigated in great details the cluster DM spectra of a system of noninteracting spinless fermions described by the Hamiltonian

$$H = -t \sum_{\langle i,j \rangle} c_i^\dagger c_j. \quad (3.1)$$

Instead of the general formalism presented in Section II A, we calculate the cluster DM weights using the exact formula

$$\rho_C = \det(1 - G_C) \exp \left\{ \sum_{i,j} [G_C(1 - G_C)]_{ij} c_i^\dagger c_j \right\} \quad (3.2)$$

obtained in Ref. 10, which relates the DM ρ_C of a cluster of sites and the cluster Green-function matrix G_C , whose matrix elements are given by

$$G_C(\mathbf{R}, \mathbf{R}') = \langle \Psi | c_{\mathbf{R}}^\dagger c_{\mathbf{R}'} | \Psi \rangle = \frac{1}{N} \sum_{\mathbf{k} \text{ filled}} e^{i\mathbf{k} \cdot (\mathbf{R} - \mathbf{R}')}, \quad (3.3)$$

where $|\Psi\rangle$ is the ground state of the system, and \mathbf{R} , \mathbf{R}' are sites within the cluster. The corollary of (3.2) is that, if λ_l is an eigenvalue of the cluster Green-function matrix G_C , the corresponding one-particle weight of ρ_C is

$$w_l = \lambda_l \prod_{l' \neq l} (1 - \lambda_{l'}). \quad (3.4)$$

With the aid of the exact formula (3.2) between the cluster DM ρ_C and the cluster Green-function matrix G_C , we can easily calculate the infinite-system spectra of ρ_C , by converting the sum in (3.3) into an integral over \mathbf{k} . However, to better understand how we can tease information regarding the infinite system out of finite systems, and also to make the comparison between noninteracting and strongly-interacting systems more meaningful (as we can only treat small systems in the latter case), we do not do this. Instead, for a finite system of N sites with P noninteracting particles, we determine the set of wave vectors $\{\mathbf{k}_n\}_{n=1}^P$ with the lowest single-particle energies

$$\epsilon_{\mathbf{k}_n} = -(\cos k_{n,x} + \cos k_{n,y}), \quad (3.5)$$

and evaluate the finite-system cluster Green-function matrix elements by summing over these occupied wave vectors in (3.3).

This give rise to cluster DM spectra contaminated by various finite size effects, which we look into in Section III A. Presumably, these same finite size effects will also arise when we exactly diagonalize finite systems of interacting fermions. As expected, finite size effects become less and less important as the size of the system is increased. Nevertheless, we still need to go to system sizes of a few hundred sites to get a decent approximation of the infinite-system cluster DM spectra. Such sizes are not practical for exactly diagonalizing the strongly-interacting system, and so we look into the method of twist boundary conditions averaging in Section III B. This allows us to calculate the cluster DM spectra for an ensemble of small finite systems, and therefrom extract the infinite system limit. We found the performance of this averaging apparatus to satisfactorily approximate the infinite-system limit cluster DM spectra for noninteracting systems.

A. Finite Size Effects and the Infinite-System Limit

Imposing the usual periodic boundary conditions, we calculated the spectrum of ρ_C for several small systems ranging from 13 to 20 sites. For these small systems sizes, we find that it is impossible to say anything meaningful about the spectrum as a function of the filling fraction $\bar{n} = P/N$ because of the finite size effects. Using the relation (3.2) for noninteracting systems, we investigated the effect of system size on the spectrum of ρ_C for a series of system $(4n, -n) \times (n, 4n)$, $1 \leq n \leq 8$, with the same shape. As the system size is increased, we find that the cluster DM spectrum approaches an infinite system limit, as shown in Figure 3. For this series of systems, the infinite system limit is more or less reached at around $n = 4$ (272 sites), judging from the convergence of the one-particle weights. We find also that the shell effect affects weights of different symmetry differently: w_{s_1} is almost unaffected, while w_d is the most severely affected.

Shell effect persists in w_d even up to a system size of 1088 sites (for $n = 8$).

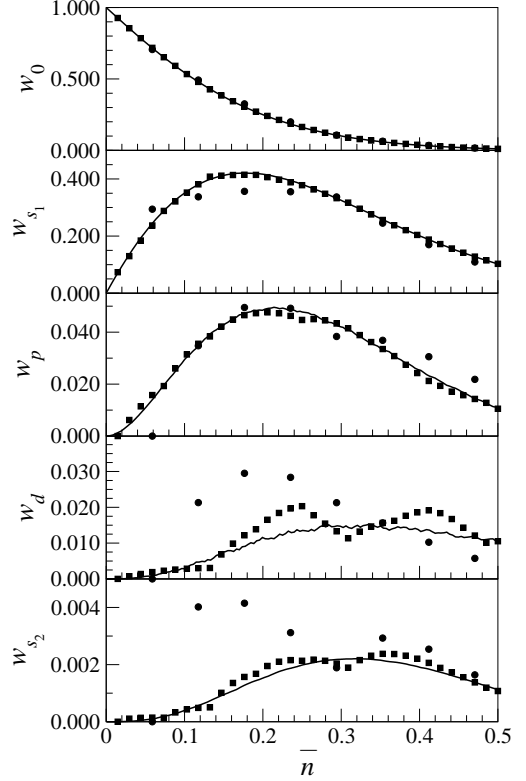


FIG. 3: Zero- and one-particle weights of the cluster DM of a 5-site, cross-shaped cluster for systems of noninteracting spinless fermions with periodic boundary conditions imposed. The systems, $(32, -8) \times (8, 32)$ (solid line), $(4, -1) \times (1, 4)$ (●), and $(8, -2) \times (2, 8)$ (■) have the same shape but different sizes. For w_{s_1} , we see the finite domain effect deviations for the $(4, -1) \times (1, 4)$ system is practically gone by the time we get to the $(8, -2) \times (2, 8)$ system. For the rest of the one-particle weights, the finite domain effect is largely removed in the $(8, -2) \times (2, 8)$ system, but shell effect persists. In fact, shell effect is still visible in the $(32, -8) \times (8, 32)$ system.

We also looked at $w_{s_1}(\bar{n})$, which is almost unaffected by shell effect, for several systems with between 200 to 300 sites of different shapes. For systems of these sizes, the finite domain effect is negligible, but we find small deviations between $w_{s_1}(\bar{n})$ from systems of different shapes. Since we expect systems of different shapes to have the same infinite system limit in principle, we attribute these deviations to the shape effect. Shape effect deviations cannot be removed by the three averaging devices we have introduced in Section II C, but fortunately these deviations are small.

B. Twist Boundary Conditions Averaging

When an analytical formula is available, as is the case for a system of noninteracting spinless fermions, there

is always the option of going to very large system sizes to determine the infinite-system limit for the spectrum of ρ_C . For a system of strongly-interacting spinless fermions, this option is not available, and twist boundary conditions averaging is the best that we can do. We need to demonstrate, using the noninteracting system as a test case, that the method of twist boundary conditions average is a reliable technique to reduce the finite domain and shell effects, using an ensemble of finite-system spectra.

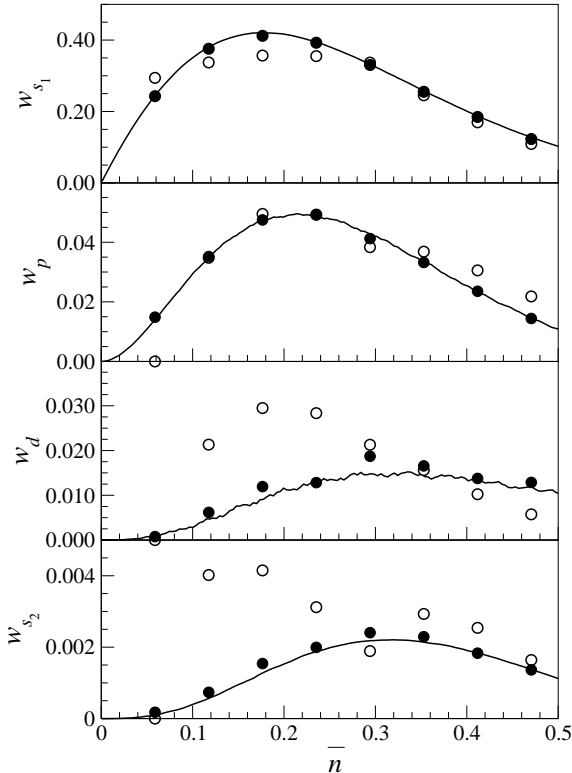


FIG. 4: One-particle weights of the cluster DM of a 5-site, cross-shaped cluster within systems of noninteracting spinless fermions. The performance of twist boundary conditions averaging, using $q = 16$ Monkhorst-Pack special-point integration, in reducing finite size effects for the $(4, -1) \times (1, 4)$ system (●) is checked against the $(4, -1) \times (1, 4)$ (○) and the $(32, -8) \times (8, 32)$ (solid line) systems with periodic boundary conditions imposed.

From our detailed study of the twist surface $\langle \Psi(\phi_x, \phi_y) | O | \Psi(\phi_x, \phi_y) \rangle$ of a generic observable O , where $|\Psi(\phi_x, \phi_y)\rangle$ is the many-body ground state of a finite system of N sites subject to twist boundary conditions with twist vector $\phi = (\phi_x, \phi_y)$, we know that there are cusps and cuts on the twist surface. For non-square systems, these cusps and cuts demarcate features with a hierarchy of sizes on the twist surface. The ‘typical’ twist surface feature has a linear dimension of $2\pi/\sqrt{N}$. These are decorated by fine structures with linear dimension $2\pi/N$, which are in turn decorated by hyperfine structures with linear dimensions $2\pi/N^2$. The number of integration points we choose to use is therefore determined

by what feature size we want to integrate faithfully.

For the purpose of this study, we decided to integrate the fine structure on the twist surface faithfully. Therefore, we chose to average the spectrum of ρ_C over a $q = 16$ Monkhorst-Pack grid (which consists of 256 integration points in the First Brillouin Zone) for the $(4, -1) \times (1, 4)$ system with $N = 17$ sites. We find that twist boundary conditions averaging does indeed result in an averaged spectrum which approximates the infinite-system limit well (see Fig. 4). This averaging device, however, does not completely eliminate shell effects, as can be seen from the twist boundary conditions-averaged $w_d(\bar{n})$. To reduce the bias this creates for one particular choice of finite system, we combined the twist boundary conditions-averaged spectrum of ρ_C for various finite systems. This is shown in Fig. 5. We now have reliable benchmarks for comparing the results of the calculations on the strongly-interacting system against.

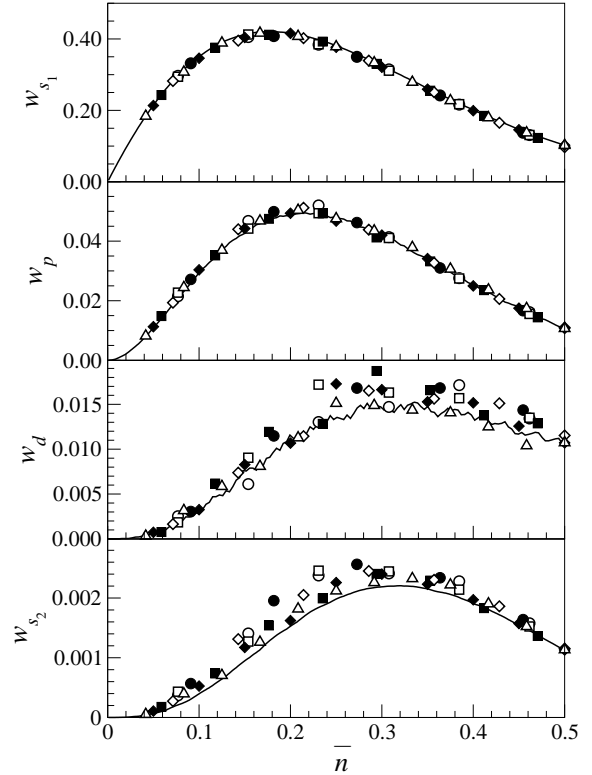


FIG. 5: One-particle weights of the cluster DM of a 5-site, cross-shaped cluster, for the $(3, -2) \times (2, 3)$ (●), $(4, 1) \times (1, 3)$ (○), $(4, -1) \times (1, 3)$ (□), $(4, -1) \times (1, 4)$ (■), $(4, -1) \times (2, 3)$ (◊), $(4, -2) \times (2, 4)$ (♦) and $(5, 1) \times (1, 5)$ (△) systems of noninteracting spinless fermions subject to twist boundary conditions averaging, using $q = 16$ Monkhorst-Pack special-point integration. Also shown is the $(32, -8) \times (8, 32)$ (solid line) system subject to periodic boundary conditions.

IV. STRONGLY-INTERACTING SYSTEM

As explained in Section I, our interest in studying the strongly-interacting model (1.1) of spinless fermions with infinite nearest-neighbor repulsion is to check whether its expected Fermi-liquid behaviour will be manifest in the structure of its cluster DM. Based on our exact result in Ref.10 for noninteracting fermions, the cluster DM for a Fermi liquid should be the exponential of a non-interacting pseudo-Hamiltonian. For a cluster DM with such a structure, the multi-particle eigenstates and multi-particle weights are all products of the one-particle eigenstates and one-particle weights respectively.

While we do not expect the zero-, one- and two-particle cluster DM weights of the strongly-interacting system, presented in Sections IV A, IV B and IV C respectively, to have the same dependence on the filling fraction \bar{n} as those of a noninteracting system, we checked whether it is possible to: (i) write the two-particle eigenstates as the product of one-particle eigenstates; and (ii) predict the relative ordering of the two-particle weights based on the relative ordering of the one-particle weights. These two criteria, when met, forms the basis of an Operator-Based DM Truncation Scheme described in Ref.6. Based on the results in Section IV B and Section IV C, we discuss the prospect of designing such a truncation scheme for the strongly-interacting system, at some or all filling fraction \bar{n} .

A. Zero-Particle Cluster Density Matrix Weight

The zero-particle cluster DM weight calculated for various finite strongly-interacting systems is shown in Fig. 6. Also shown in the figure is the zero-particle cluster DM weight of the noninteracting $(32, -8) \times (8, 32)$ system. As we can see, the zero-particle weights of the respective systems only start differing significantly from each other for $\bar{n} > 0.1$. With repulsive interacting between spinless fermions, it is more difficult in a congested system ($\bar{n} > 0.2$) to form an empty cluster of sites from quantum fluctuations. As a result, the strongly-interacting w_0 falls below the noninteracting w_0 . However, this fact alone does not tell us anything more about the correlations in the strongly-interacting ground state, and so we move on to consider the one-particle cluster DM weights.

B. One-Particle Cluster Density Matrix Eigenstates and Their Weights

As explained in Section I, we calculate the spectra of the cluster DM for the strongly-interacting system to examine how much of the Operator-Based DM Truncation Scheme, developed in Ref.6 for a noninteracting system, can be applied to a strongly-interacting one. In this section, we present results for a series of calculations to de-

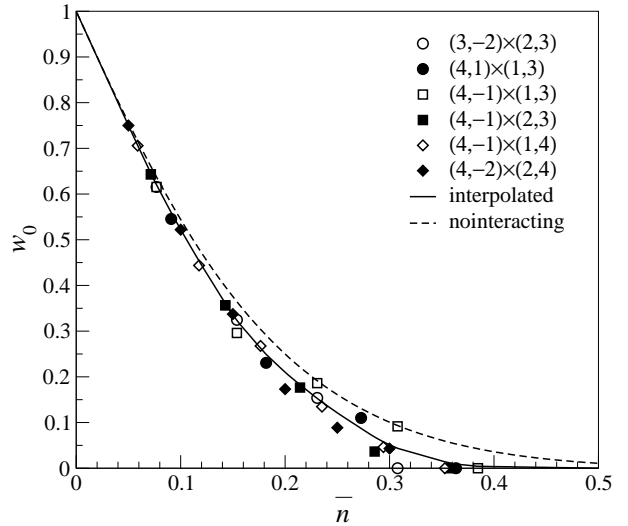


FIG. 6: Zero-particle weight of the cluster DM of a 5-site, cross-shaped cluster, for the $(3, -2) \times (2, 3)$ (\bullet), $(4, 1) \times (1, 3)$ (\circ), $(4, -1) \times (1, 3)$ (\square), $(4, -1) \times (1, 4)$ (\blacksquare), $(4, -1) \times (2, 3)$ (\lozenge) and $(4, -2) \times (2, 4)$ (\blacklozenge) systems of strongly-interacting spinless fermions subject to twist boundary conditions averaging, using $q = 8$ Monkhorst-Pack special-point integration. At $\bar{n} = 0$ and $\bar{n} = \frac{1}{2}$, we know analytically that $w_0 = 1$ and $w_0 = 0$ respectively, and the solid ‘curve’ interpolates between these two known limits and the equally weighted data points at finite filling fractions $0 < \bar{n} < \frac{1}{2}$. Also shown as the dashed curve is the zero-particle weight of the $(32, -8) \times (8, 32)$ (solid line) system of noninteracting spinless fermions subject to periodic boundary conditions.

termine the infinite-system limit of the one-particle cluster DM spectra for our strongly-interacting system as a function of filling fraction \bar{n} , before going on to discuss the applicability of the Operator-Based DM Truncation Scheme.

Though we really do need to worry about the evolution of the structure of $|s_1\rangle$ and $|s_2\rangle$ as a function of \bar{n} in both the noninteracting and strongly-interacting systems, the one-particle weights are ordered by their magnitudes as $w_{s_1} > w_p > w_d > w_{s_2}$ for both systems. But while the noninteracting one-particle weights go down by roughly one order of magnitude as we go through the sequence $w_{s_1} \rightarrow w_p \rightarrow w_d \rightarrow w_{s_2}$, we see from Fig. 7 that the interacting one-particle weights decay more slowly along this same sequence.

We studied the finite $(3, -2) \times (2, 3)$ (\bullet), $(4, 1) \times (1, 3)$ (\circ), $(4, -1) \times (1, 3)$ (\square), $(4, -1) \times (1, 4)$ (\blacksquare), $(4, -1) \times (2, 3)$ (\lozenge) and $(4, -2) \times (2, 4)$ (\blacklozenge) systems subject to twist boundary conditions averaging, using $q = 8$ Monkhorst-Pack special-point integration. At a filling fraction of $\bar{n} = 0$, the system approaches the noninteracting limit, and thus all the one-particle weights are zero. At half-filling $\bar{n} = \frac{1}{2}$, the two-fold degenerate checker-board ground state is unaffected by twist boundary conditions averaging. We can thus perform degeneracy averaging analyt-

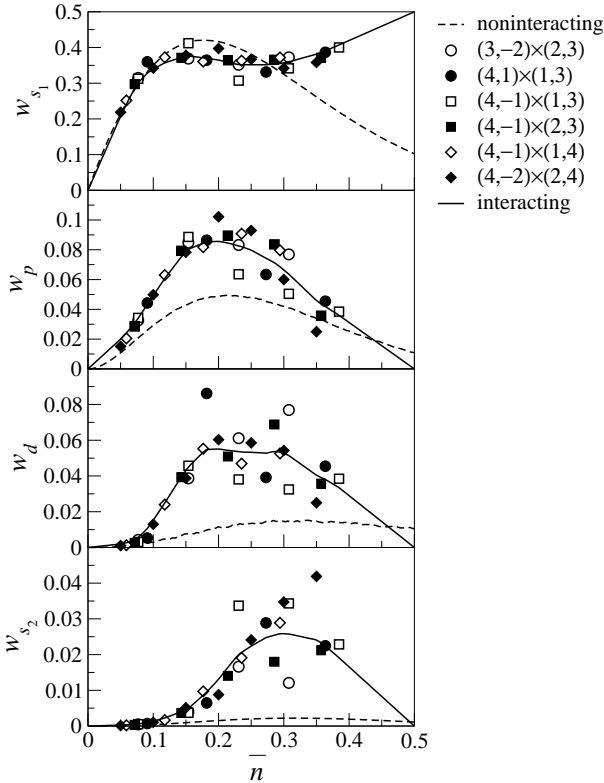


FIG. 7: One-particle weights of the cluster DM of a 5-site, cross-shaped cluster within a system of strongly-interacting spinless fermions.

ically, to find that $w_{s_1} = \frac{1}{2}$ and $w_p = w_d = w_{s_2} = 0$. The solid ‘curves’ in Figure 7 interpolate between these two known limits and the equally weighted data points at finite filling fractions $0 < \bar{n} < \frac{1}{2}$. Also shown in Figure 7 as the dashed curves are the one-particle weights of the noninteracting $(32, -8) \times (8, 32)$ (solid line) system subject to periodic boundary conditions.

In an Operator-Based DM Truncation Scheme, we discard one-particle cluster DM eigenstates with very small weights, and keep only the many-particle cluster DM eigenstates built from the retained one-particle eigenstates. The sum of weights of the truncated set of cluster DM eigenstates will then be very nearly one, if the discarded one-particle weights are all very small compared to the maximum one-particle weight. As we can see from Fig. 7, the ratio of the largest one-particle weight, w_{s_1} , to the smallest one-particle weight, w_{s_2} , is not large enough for us to justify keeping $|s_1\rangle$ and discarding $|s_2\rangle$, except when the system is very close to half-filled. This calls into question the validity, or value, of the truncation scheme.

C. Two-Particle Eigenstates and Weights

Of the two-particle states listed in (2.31), the only states which are allowed by the no-nearest-neighbor con-

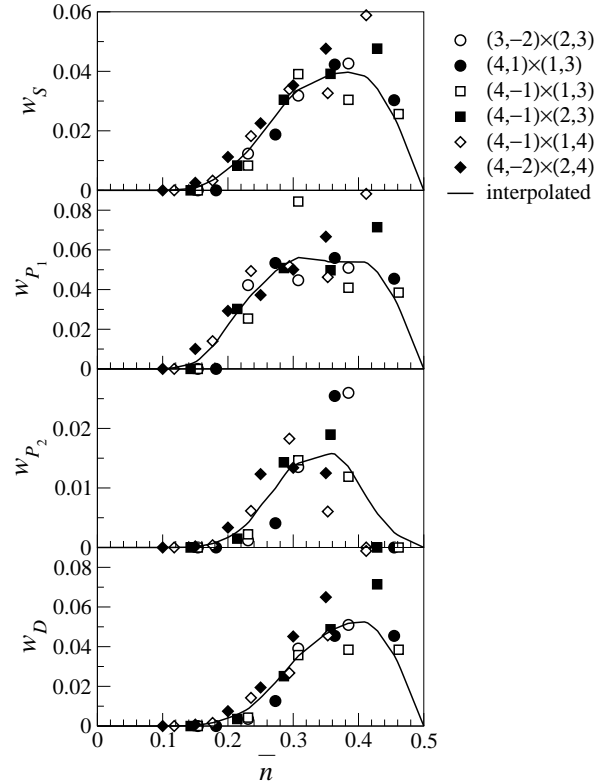


FIG. 8: Two-particle weights of the cluster DM of a 5-site, cross-shaped cluster within a system of strongly-interacting spinless fermions.

straint to appear in the cluster Hilbert space are $|S\rangle$, $|P_{\pm}\rangle$, $|P''_{\pm}\rangle$ and $|D\rangle$. We know therefore that the two-particle sector of ρ_C comprises a 1×1 S -diagonal block (with weight w_S), a 1×1 D -diagonal block (with weight w_D), and two degenerate 2×2 P -diagonal blocks (with weights w_{P_1} and w_{P_2}). The two-particle weights are shown as a function of filling \bar{n} in Fig. 8.

For the finite $(3, -2) \times (2, 3)$ (●), $(4, 1) \times (1, 3)$ (○), $(4, -1) \times (1, 3)$ (□), $(4, -1) \times (1, 4)$ (■), $(4, -1) \times (2, 3)$ (◊) and $(4, -2) \times (2, 4)$ (◆) systems studied, subject to twist boundary conditions averaging, using $q = 8$ Monkhorst-Pack special-point integration, all the two-particle weights are zero at $\bar{n} = 0$ as the systems approach the noninteracting limit. At half-filling $\bar{n} = \frac{1}{2}$, we again perform degeneracy averaging analytically on the two-fold degenerate checker-board ground state to find that all the two-particle weights are zero. In Figure 8, the solid ‘curves’ interpolate between these two known limits and the equally weighted data points at finite filling fractions $0 < \bar{n} < \frac{1}{2}$.

There are significantly fewer nontrivial two-particle eigenstates of ρ_C than predicted by the combination of one-particle eigenstates. This poses no problem to our Operator-Based DM Truncation Scheme, if the non-occurring two-particle states are predicted to have small enough weights that they will be excluded by the truncation scheme.

tion scheme. However, we find that this is not the case. For example, the two-particle state $|S'\rangle$, which does not occur, is predicted by simple combination of the one-particle states $|s\rangle$ and $|\bar{s}\rangle$ to have a weight comparable to that of the two-particle state $|S\rangle$, which does occur. This means that if we are to push the Operator-Based Density-Matrix Truncation Scheme through, we cannot do so naively.

Of the two-particle weights that are allowed by the no-nearest-neighbor constraint, we expect their weights to follow the sequence $w_{P_1} \gtrsim w_D > w_S$, if they can indeed be thought of products of one-particle states. From Fig. 8, we indeed observe this sequence of two-particle weights, even though their actual magnitudes (calculated as the product of one-particle weights divided by the zero-particle weight) do not come out right.

V. SUMMARY & DISCUSSIONS

To summarize, we have calculated numerically the cluster DM for a cross-shaped cluster of five sites within both a system of noninteracting spinless fermions described by the Hamiltonian (3.1), and a system of strongly-interacting spinless fermions described by the Hamiltonian (1.1). The cluster DM is first obtained from the exact-diagonalization ground-state wave function by tracing down degrees of freedom outside of the cluster. Full square-lattice symmetry in the cluster DM is then restored by performing degeneracy averaging followed by orientation averaging.

Analyzing finite systems of noninteracting spinless fermions, we find the numerical spectra of cluster density matrices so obtained to be plagued by finite size effects. By increasing the system size systematically, we find a unique and unambiguous infinite-system limit for the cluster DM spectra, but that this is approached by finite systems with a couple of hundred sites. These are forbiddingly large system sizes for interacting systems, whose ground-state wave functions have to be obtained via exact diagonalization.

We then tested the apparatus of twist boundary conditions averaging on finite systems with between 10 and 20 sites. For noninteracting spinless fermions, we find that the twist boundary conditions-averaged weights for different systems and different filling fractions fall onto various smooth curves. This assures us that twist boundary conditions averaging practically eliminates finite size effects, and the cluster DM approaches that obtained from the ground-state wave function of an infinite square lattice.

Comparing the twist boundary conditions-averaged cluster DM spectra for the noninteracting and strongly-interacting systems, we find that the zero-particle weights w_0 for the noninteracting and strongly-interacting systems have the same qualitative behaviour, except for the fact that w_0 for the strongly-interacting system falls sig-

nificantly below that of the noninteracting system, for $\bar{n} > 0.1$, because of the smaller likelihood to find configurations containing a cross-shaped cluster of five empty sites as \bar{n} increases when the spinless fermions repel each other. The one-particle weights w_{s_1} , w_p , w_d and w_{s_2} are qualitatively different for the two system types, even though the relative ordering $w_{s_1} > w_p > w_d > w_{s_2}$ is the same. But while the one-particle weights go down by roughly one order of magnitude each time as we go through the sequence $w_{s_1} \rightarrow w_p \rightarrow w_d \rightarrow w_{s_2}$ in the noninteracting system, this decay is much slower in the strongly-interacting system.

The implications of this observation to the Operator-Based DM Truncation Scheme developed in Ref. 6 is that, for a small fixed fraction of one-particle eigenstates retained, the total cluster DM weight of eigenstates retained would be much smaller for the strongly-interacting system compared to the noninteracting system. However, as shown in Ref. 6, we need to calculate other observables, such as the dispersion relation, before we can say for sure how badly the numerical accuracy of the truncation scheme is affected by the fact that the ratio of the smallest to the largest one-particle weights, w_{s_2}/w_{s_1} , is not very much smaller than one.

However, for the retained one-particle cluster DM eigenstates to furnish a good ‘quasi-particle’ description for the strongly-interacting system, the many-particle eigenstates must be reasonably well represented by combinations of one-particle eigenstates. For the two-particle cluster DM eigenstates, we find far too many two-particle states generated by taking combinations of one-particle eigenstates. Most of these combinatorial two-particle states are invalid, because of the restriction imposed by (1.1) on nearest neighbor occupation. This is not a debilitating problem, because we can always build restrictions into the Operator-Based DM Truncation Scheme to have these invalid states removed. More importantly, based on the valid two-particle combinations, we predict that $w_{P_1} \gtrsim w_D > w_S$ for the three of the four distinct two-particle cluster DM weights, which is indeed what we observe numerically, even though the predicted weights are off.

With these checks, we conclude that it may be possible to implement a modified Operator-Based DM Truncation Scheme on a strongly-interacting system, notwithstanding the possibility that the structure of the interacting cluster DM may not lend itself to an adequate description in terms of independent ‘quasi-particle’ operators. We are less optimistic about the performance of such a truncation scheme in the strongly-interacting system, for two reasons. Firstly, the ratio of the maximum one-particle weight to the minimum one-particle weight is not large enough to justify keeping one and throwing the other away. Secondly, and more critically, the many-particle weights cannot be reliably calculated from the zero- and one-particle weights. This means that we have very little control over the computational accuracy of observables

calculated using the truncation scheme, for a given computational time expenditure. This reward-to-effort ratio is an important factor in helping us decide how much compromise we need to make in terms of accuracy of the final result versus the time needed to acquire it.

Acknowledgments

This research is supported by NSF grant DMR-0240953, and made use of the computing facility of the

Cornell Center for Materials Research (CCMR) with support from the National Science Foundation Materials Research Science and Engineering Centers (MRSEC) program (DMR-0079992). SAC would like to thank Garnet Chan for illuminating discussions on the numerical implementation of the trace-down algorithm.

¹ S. R. White, Phys. Rev. Lett. **69**, 2863 (1992); Phys. Rev. B **48**, 10345 (1993).

² F. Verstraete, D. Porras, and J. I. Cirac, Phys. Rev. Lett. **93**, 227205 (2004); F. Verstraete and J. I. Cirac, cond-mat/0407066 (2004).

³ S. Capponi, A. Läuchli, and M. Mambrini, Phys. Rev. B **70**, 104424 (2004).

⁴ S. Furukawa, G. Misguich, and M. Oshikawa, cond-mat/0508469 (2005).

⁵ M. C. Chung and I. Peschel, Phys. Rev. B **64**, 064412 (2001).

⁶ S.-A. Cheong and C. L. Henley, Phys. Rev. B **69**, 075112 (2004).

⁷ C. L. Henley and N. G. Zhang, Phys. Rev. B **63**, 233107 (2001).

⁸ N. G. Zhang and C. L. Henley, Phys. Rev. B **68**, 014506 (2003).

⁹ N. G. Zhang and C. L. Henley, Eur. Phys. J. B **38**, 409 (2004).

¹⁰ S.-A. Cheong and C. L. Henley, Phys. Rev. B **69**, 075111 (2004).

¹¹ S.-A. Cheong, Ph.D. thesis, Cornell University (in preparation).

¹² G. Spronken, R. Jullien and M. Avignon, Phys. Rev. B **24**, 5356 (1981); X. Zotos, P. Prelovšek and I. Sega, Phys. Rev. B **42**, 8445 (1990); D. Poilblanc and E. Dagotto, Phys. Rev. B **44**, 466 (1991); D. Poilblanc, Phys. Rev. B **44**, 9562 (1991); C. Gros, Z. Phys. B – Condensed Matter **86**, 339 (1992); J. T. Gammel, D. K. Campbell and E. Y. Loh, Jr., Synth. Met. **57**, 4437 (1993); C. Lin, F. H. Zong, and D. M. Ceperley, Phys. Rev. B **64**, 016702 (2001).

¹³ H. J. Monkhorst and J. D. Pack, Phys. Rev. B **13**, 5188 (1976); D. J. Chadi, Phys. Rev. B **16**, 1746 (1977); J. D. Pack and H. J. Monkhorst, Phys. Rev. B **16**, 1748 (1977).

¹⁴ Eric W. Weisstein. “Dihedral Group D4.” From *MathWorld* — A Wolfram Web Resource, <http://mathworld.wolfram.com/DihedralGroupD4.html>; M. Lax, *Symmetry Principles in Solid State and Molecular Physics* (Dover (Mineola, New York), 2001); J. M. Hollas, *Modern Spectroscopy, Third Edition* (John Wiley & Sons (Chichester), 1996).